


## Thermoresponsive mobility of liquid crystals and reactive mesogens during photopolymerization-induced phase separation

Hiroshi Kakiuchida <sup>1,\*</sup>, Akihiko Matsuyama,<sup>2</sup> Eiichi Kobayashi,<sup>3</sup> and Akifumi Ogiwara<sup>4</sup>

<sup>1</sup>*Innovative Functional Materials Research Institute, National Institute of Advanced Industrial Science and Technology, Nagoya 463-8560, Japan*

<sup>2</sup>*Faculty of Computer Science and Systems Engineering, Kyushu Institute of Technology, Iizuka 820-8502, Japan*

<sup>3</sup>*Kyushu Synchrotron Light Research Center, Tosu 841-0005, Japan*

<sup>4</sup>*Department of Electronic Engineering, Kobe City College of Technology, Kobe 651-2194, Japan*



(Received 20 May 2022; accepted 27 September 2022; published 20 October 2022)

Molecular interactions between liquid crystals (LCs) and reactive mesogens (RMs) at temperatures across the phase transition regions were comprehensively studied during photopolymerization-induced phase separation (PPIPS) beginning with raw mixtures until the formation of polymer network liquid crystals (PNLCs). Then, the molecules were found to be nonuniformly more and less mobile in response to temperature as PPIPS progressed. Optical birefringence and infrared absorption were carefully measured throughout PPIPS, using 4-cyano-4'-hexylbiphenyl (6CB) and 1,4bis-[4-(3-acryloyloxypropyloxy) benzoyloxy]-2-methylbenzene (RM257) as typical LCs and RMs. Microscopic views of thermoresponsive changes in the molecular orientation order of both LCs and RMs were obtained: LCs and RMs in raw mixtures interacted with one another but uniformly transformed their molecular orientation. Such interactions continuously change to become nonuniform with progress in PPIPS. At the incipient stages of PPIPS, RMs, which are polymerized but not completely networked, inhibit LCs from changing their molecular orientation and vice versa. As PPIPS progresses, some LCs become more mobile and some less mobile owing to RM constraints. The domain configuration of the submicrometer phase separation affects the thermoresponsive mobility of LCs and RMs, that is, LCs become more mobile in LC-rich areas. The quantitative knowledge here provides comprehensive insight that LCs and RMs are mutually constrained and that such interactive behavior varies nonuniformly as PPIPS progresses.

DOI: [10.1103/PhysRevE.106.044704](https://doi.org/10.1103/PhysRevE.106.044704)

### I. INTRODUCTION

Liquid crystals (LCs) coexisting with monomers and polymers, which have a ternary structure while forming polymer network liquid crystals (PNLCs), are mutually constrained in different manners depending on the progress of the self-assembly process, called polymerization-induced phase separation (PIPS) [1,2]. The complex behavior of such interactive molecules has been studied extensively not only because of its interest to soft-matter physics, such as miscibility and liquid–liquid (or liquid–solid or polymer–polymer) phase separation [1,3,4], but also because of their indispensability for technological applications [5–8]. In particular, mixtures of LCs with reactive mesogens (RMs), which possess an anisotropic rigid body such as LCs, along with reactive groups, have received much attention from the aspect of stimuli-responsive interactions between nonpolymerizable and polymerizable anisotropic molecules during PIPS. Intuitively, the molecular orientation of LCs in PNLCs, which are more narrowly confined or strongly entangled by polymers, is harder to rearrange by the nematic-to-isotropic (NI) phase transition. The structure of the polymer networks surrounding LCs can influence macroscopic properties under extrinsic

stimuli, such as electro- and thermo-optical properties. The threshold fields to change the light transmittance tend to be higher for smaller domains of the LC phase formed in PNLCs [9–12]. The NI phase transition temperature ( $\tau_{NI}$ ) is also influenced by polymer networks, that is,  $\tau_{NI}$  becomes higher for LCs that are more closely confined in the polymer networks [9,13].

While PNLCs are formed, LCs and polymers are mutually affected in different ways depending on the progress in PIPS. Particularly, the interactions of LCs with RMs are complicated. Both have mesogenic bodies and exhibit individual anisotropic properties, such as birefringence and molecular orientation order. RMs and LCs form various distributions of molecular orientation at different stages before, during, and after PIPS. Ternary systems of LCs and RMs before and after polymerization potentially form various distributions in phase separation and molecular orientation order, depending on the progress of PIPS. The interaction of LCs with polymers during PIPS has been extensively studied using numerical simulations and experiments [14,15]. Blonski *et al.* [16] discussed the miscibility of LC polymers, isotropic polymers, and solvents based on Flory-based theories, and the orientation order of the LCs was found to depend on the distance from the solvent to the LCs. Boots *et al.* [17] calculated the free energy at different stages of thermally induced phase separation (TIPS) and then exhibited phase diagrams for ternary

\*h.kakiuchida@aist.go.jp

systems of monomers, polymers, and LCs during polymerization. The numerical simulation by Kyu *et al.* clearly visualized the formation of domains and ordering of molecular orientation through PIPS, based on a free-energy model determined by the Flory-Huggins and Maier-Saupe theories. The simulation showed a correlation between the molecular distribution and orientation order of LCs at different stages of PIPS [18,19]. The microscopic view of the interactions between different types of mesogenic molecules in mixtures is intriguing. Phase diagrams of a mixture of two different LCs were obtained by calculating the free energy based on the Flory-Huggins interaction theory [20]. Binary mixtures of rodlike and bent-core LCs were observed by polarizing optical microscopy (POM), and the microtextures generated depending on thermal process were discussed considering the viscoelastic properties of these two different LCs [21]. Some research groups have produced elaborate structures composed of LCs and RMs. One study produced mesoscale composites of nematic LCs around block copolymers anchored on LC polymer (LCP)-modified surfaces [22]. The molecular orientation distribution of LCs and LCPs in such structures was visually revealed using two-dimensional small-angle neutron scattering. Another group developed bicontinuous (not isolated) phases of polymerized RMs microscopically aligned with LC fluids [23]. This structure can avoid decreasing the stimuli-responsive mobility of LCs and consequently maintain excellent macroscopic electro-optical switchability. Cyanobiphenyl LCs and main-chain ester diacrylate RMs are typical composites of PNLCs because of their practical and extensive applicability. These phase diagrams were obtained before and after photopolymerization-induced phase separation (PPIPS) by POM and thermal analyses, and discussed based on the Maier-Saupe and Flory-Huggins theories [24].

We created different mesoscale phase separation domains of LCs and RMs that were co-ordered in molecular orientation via PPIPS. Then, the influence of the domain distribution on the orientation-(dis)ordering of the LCs and RMs was comprehensively studied by carefully measuring the optical birefringence and infrared absorption. Our work focuses on tracking the thermoresponsive orientation-(dis)ordering of both LCs ( $S_{LC}$ ) and RMs ( $S_{RM}$ ) at different stages during PPIPS, from the raw mixtures to the PNLCs. The quantitative knowledge presented here provides comprehensive insight into the thermoresponsive behavior of typical LCs and RMs that interact in different manners depending on the progress in PPIPS.

## II. EXPERIMENT

We used mixtures of liquid crystals, reactive mesogens, photoinitiators (PIs), and co-initiators (CIs). The LCs were a nematic-type, 4-cyano-4'-hexylbiphenyl [C3154, Tokyo Chemical Industry Co., Ltd. (TCI)], called 6CB. The RMs were a main-chain ester diacrylate monomer, 1,4-bis-[4-(3-acryloyloxypropyloxy) benzoyloxy]-2-methylbenzene (RM257, Merck Corp.). The PIs were dibromofluorescein (D1120, TCI) and the CIs were N-phenylglycine (P0180, TCI) for photopolymerization under green light. The LCs and RMs were mixed at compositional ratios of  $\phi$  and  $(1-\phi)$  in wt.%, respectively, and then the PI and CI were added at 0.1 and

0.1 wt.%, respectively. The mixtures were stirred at 60 °C until becoming uniformly transparent liquids. The refractive indices of 6CB on the catalog for ordinary and extraordinary rays are  $n_o = 1.5370$  and  $n_e = 1.6918$ , respectively, and  $\tau_{NI} = 29$  °C. The physical properties of RM257 are  $n_o = 1.508$ ,  $n_e = 1.687$ , and  $\tau_{NI} = 127$  °C on the catalog. The specific gravities of 6CB and RM257 were determined to be  $\rho_{LC} = 1.026 \pm 0.011$  g/cm<sup>3</sup> and  $\rho_{RM} = 1.263 \pm 0.056$  g/cm<sup>3</sup>, respectively, by measuring their volume and weight, which agreed with the reported and calculated values [25,26].

Transparent glass substrates, the sizes of which were 25×20×0.7 and 25×20×0.1 mm, were used. The thinner substrates were used to measure infrared absorption at wave numbers less than 2000 cm<sup>-1</sup>. To stabilize the LCs and RMs ordered in molecular orientation, the surfaces were horizontally rubbing treated along the longitudinal direction of the substrates with polyimide coating (EHC Co., Ltd.). The raw mixtures were poured into a gap formed between a pair of glass substrates. The gap distance, which was necessary to obtain birefringence, was fixed at 30 μm with beads and precisely measured by optical interferometry with multiple internal reflections between the substrates, where the gap thickness was decided for a subsidiary purpose, that is, to be compared with the authors' study of thermoresponsive switchability between optical transparency and haze [7]. The raw mixtures between the glass substrates turned to PNLCs through PPIPS by photoirradiation at 20 °C for different prescribed duration at a wavelength of 532 nm and intensity of 100 mW/cm<sup>2</sup> using a Nd : YVO<sub>4</sub> laser (J150GS, Showa Optronics Co., Ltd. or GLK32300TS, LASOS Lasertechnik GmbH).

To discuss the molecular orientation order of LCs ( $S_{LC}$ ) and RMs ( $S_{RM}$ ) during PPIPS, the relationship between the molecular orientation and birefringence was determined for individual raw materials of LCs and RMs beforehand, assuming that they are proportional [27], that is,

$$S_{LC} = k_{LC} \Delta n_{LC} \quad (1)$$

and

$$S_{RM} = k_{RM} \Delta n_{RM}. \quad (2)$$

$\Delta n_{LC}$  and  $\Delta n_{RM}$  are the birefringence values of the LC and RM raw materials, respectively. The proportional coefficients  $k_{LC}$  and  $k_{RM}$  were determined by fitting the data obtained from infrared absorption spectroscopy and visible-to-near-infrared spectrophotometry at different temperatures.  $S_{LC}$  and  $S_{RM}$  were calculated individually from the infrared absorption spectra. The absorption of the peak around 2226 cm<sup>-1</sup> originates from the stretching vibrational mode of the cyano groups ( $-C \equiv N$ ) belonging to 6CB [28]. The absorption of the peak around 1606 cm<sup>-1</sup> can be attributed to a symmetric rocking vibrational mode of the *para*-disubstituted benzene rings belonging to RM257 [29]. The areas of the individual absorption peaks were measured at two orthogonal polarization azimuths, parallel ( $A_{||}$ ) and perpendicular ( $A_{\perp}$ ) to the direction of the rubbing treatment, using a Fourier-transform infrared (FTIR) spectrophotometer (Frontier, PerkinElmer Co., Ltd.) with an infrared polarizer (WP25H-C, Thorlabs Japan Inc.). Then,  $S_{LC}$  and  $S_{RM}$  were estimated to be [30]

$$S_{LC} \text{ and } S_{RM} = (A_{||} - A_{\perp}) / (A_{||} + 2A_{\perp}). \quad (3)$$

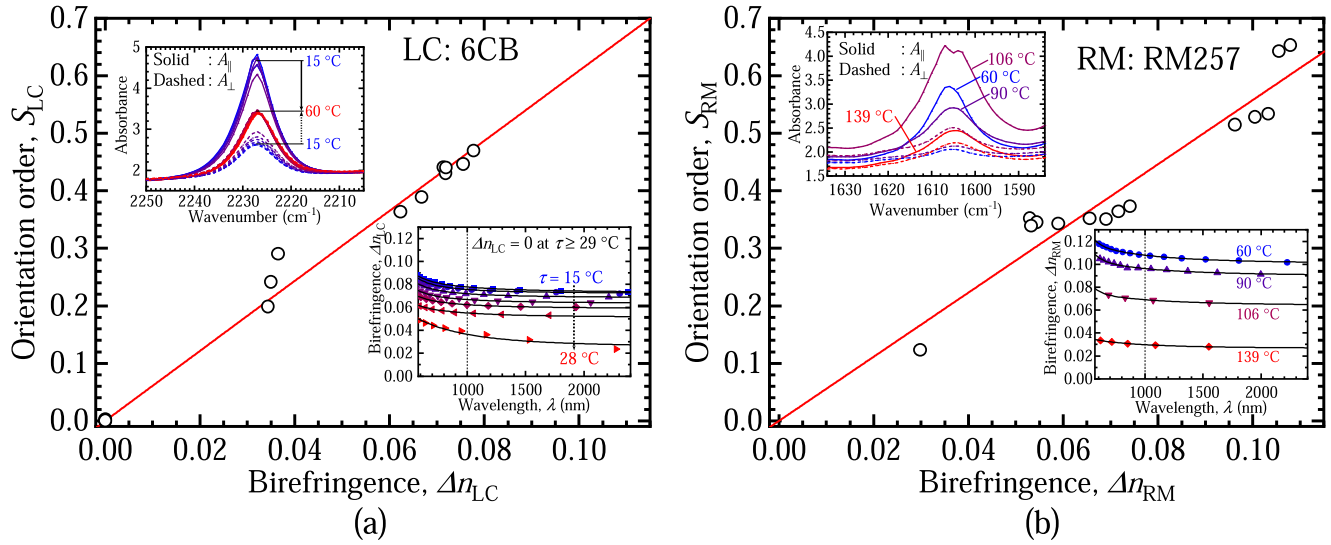


FIG. 1. Relationship between orientation order and birefringence of raw materials: (a) LCs and (b) RMs. Birefringence is the value at 1- $\mu\text{m}$  wavelength obtained by Cauchy wavelength dispersion. Circular symbols are measurements obtained at different temperatures. Upper insets show FTIR absorption peak resulting from (a) cyano groups belonging to 6CB [28] and (b) phenyl rings belonging to RM257 [29]. Lower insets show wavelength dispersion of birefringence determined by wavelengths of repetitive peaks and valleys in optical transmittance at XN state. Solid black curves indicate Cauchy wavelength dispersion.

Note that  $A_{\parallel}$  and  $A_{\perp}$  are the absorption areas around  $2226\text{ cm}^{-1}$  for  $S_{LC}$  and  $1606\text{ cm}^{-1}$  for  $S_{RM}$ .  $\Delta n_{LC}$  and  $\Delta n_{RM}$  were determined from the transmittance spectra of the raw materials of LCs and RMs individually measured using a spectrophotometer (U4100, Hitachi High-Technologies Corp.) with two polarizers in the crossed-Nicols (XN) state, that is, polarizing azimuths of  $\pm 45^\circ$  from the direction of the rubbing treatment. The transmittance of the raw materials cycles up and down as a function of wavelength if the raw materials have uniaxial optical anisotropy along the rubbing-treatment direction. The wavelengths where the repetitive peaks and valleys are located provide birefringence on the assumption that the wavelength dispersion of the birefringence obeys the four-term Cauchy equation. Figures 1(a) and 1(b) show the relationship between the orientation order and birefringence of the raw materials of the LCs and RMs, respectively, which were measured at different temperatures.  $k_{LC}$  and  $k_{RM}$  were determined to be  $6.085 \pm 0.118$  and  $5.577 \pm 0.141$ , respectively, from the slopes of the fitted lines.

The birefringence of the PNLCs ( $\Delta n_{PNLC}$ ) was measured in the same manner as  $\Delta n_{LC}$  and  $\Delta n_{RM}$  of the individual raw materials, as stated above. The additivity of the birefringence of the LC and RM phases in the mixture was employed here on the assumption that the refractive index of the mixture can be determined using an effective medium approximation [31,32]. The additivity assumption here was found to be reliable by the supplemental experiment (see Supplemental Material [33]). Thus,  $\Delta n_{PNLC}$  can be expressed by the volume average of  $\Delta n_{LC}$  and  $\Delta n_{RM}$  as follows:

$$\Delta n_{PNLC} = \phi_v \Delta n_{LC} + (1 - \phi_v) \Delta n_{RM}, \quad (4)$$

where  $\phi_v$  is the volumetric ratio of LCs in the mixture of LCs and RMs and is expressed using  $\rho_{LC}$ ,  $\rho_{RM}$ , and  $\phi$  as  $\phi / \{\phi + (\rho_{LC}/\rho_{RM})(1-\phi)\}$ .

$S_{LC}$  in the PNLCs was determined from the infrared absorption spectrum of the  $2226\text{-cm}^{-1}$  band, in the same way as in the raw material of the LCs, by Eq. (3) because this absorption peak can be deconvoluted from the others in the PNLCs. In contrast,  $S_{RM}$  in the PNLCs was determined by calculations using Eqs. (1), (2), and (4) from the measurements of  $S_{LC}$  and  $\Delta n_{PNLC}$  because the infrared absorption spectrum of the  $1606\text{-cm}^{-1}$  band was technically difficult to deconvolute, which is caused by the vibrational modes of the benzene rings in both 6CB and RM257. First,  $\Delta n_{LC}$  was estimated from the measured  $S_{LC}$  using Eq. (1). Next,  $\Delta n_{RM}$  was obtained from the estimated  $\Delta n_{LC}$  and measured  $\Delta n_{PNLC}$  using Eq. (4). Then,  $S_{RM}$  was determined from the estimated  $\Delta n_{RM}$  using Eq. (2).

The degree of conversion,  $m$ , was determined by examining the decrease in the absorption area,  $\alpha$ , of the  $1635\text{-cm}^{-1}$  band. This absorption arises from the stretching vibrational mode of carbon double bonds ( $-\text{C}=\text{C}-$ ) in acryloyl groups [34,35], and provides  $m$  as

$$m = 1 - \alpha/\alpha_0, \quad (5)$$

where  $\alpha_0$  is the value of  $\alpha$  before photopolymerization. Figure 2 shows the absorption around  $1635\text{ cm}^{-1}$  at different stages of photopolymerization, where the samples were photoirradiated until the polymerization stagnated. The peak area decreased as photopolymerization progressed.

Phase separation structures were observed at  $20\text{ }^\circ\text{C}$  and  $50\text{ }^\circ\text{C}$ , using a polarizing optical microscope (POM; MT9430, Meiji Techno Co., Ltd.) in the XN state with two polarizers sandwiching the sample, one set at a polarization azimuth of  $+45^\circ$  from the rubbing direction, and the other set at  $-45^\circ$ . The samples were sliced into cross sections and rinsed with methanol to remove the LCs. The remaining phase separation

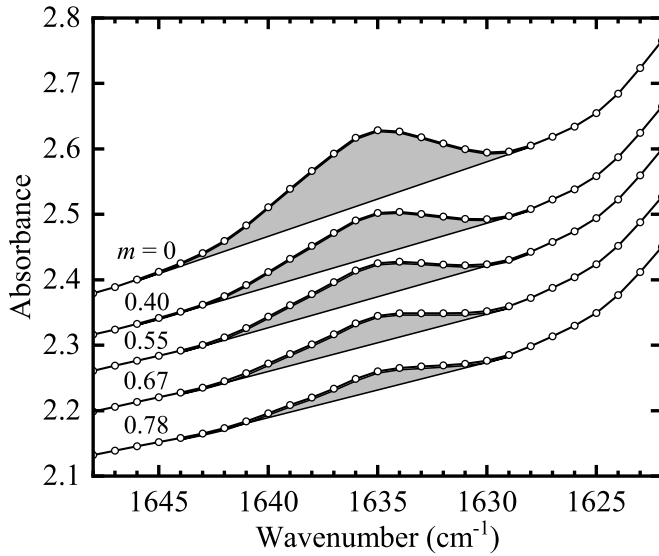


FIG. 2. Infrared absorption spectra of the 1635-cm<sup>-1</sup> band for different degrees of conversion in raw mixture of 6CB and RM257, originating from a stretching vibrational mode of carbon double bonds belonging to acryloyl groups in RM257 [33,34]. Absorption area of the band ( $\alpha$ ), as expressed in Eq. (5), was calculated between spectral curve and baseline tangent to curve, as shown by gray highlight.

structures were observed using scanning electron microscopy (SEM; S-4300, Hitachi High-Technologies Corp.).

### III. RESULTS

The PNLC samples were prepared at three different weight ratios:  $\phi = 0.64, 0.70,$  and  $0.80$ . Figures 3 and 4 show POM and SEM images of the three samples, respectively. All the

samples thermoresponsively changed optical anisotropy, as shown by the different colors depending on temperatures between 20 °C and 50 °C in the POM images in Fig. 3. The images at 20 °C were uniformly brown at the XN state at polarizing azimuths of  $\pm 45^\circ$  from the direction of the rubbing treatment and dark (slightly nonuniform) at the XN state at polarizing azimuths of  $0^\circ$  and  $90^\circ$ , independent of  $\phi$ , whereas those at 50 °C showed a nonuniform color distribution that depended on  $\phi$ , as shown in Figs. 3(a)–3(c). The uniformly bright and dark images at the XN states at  $\pm 45^\circ$  and at  $0^\circ/90^\circ$ , respectively, suggest that LC and RM molecules in the PNLCs were co-ordered in molecular orientation along the rubbing-treatment direction. The cross sections of the polymer phase exhibited different configurational features of submicrometer dimensions depending on  $\phi$ , that is, it appeared rugged, reticular, and grainy with the increase in  $\phi$ , as shown in Figs. 4(a)–4(c), respectively. The polymer structures were uniform along the thickness direction, according to the whole views of the cross sections, as shown in the inset images.

$S_{LC}$  was measured as a function of temperature,  $\tau$ , at different stages in the PPIPS ( $m = 0, 0.55,$  and  $0.78$ ), as shown in Fig. 5. Before PPIPS ( $m = 0$ ),  $S_{LC}$  decreased and reached zero as  $\tau$  increased. This decrease exhibits a typical NI transition and was fitted to a power-law function of  $\tau$ ,

$$S_{LC} = A(T_0 - \tau)^B, \quad (6)$$

as shown by the black solid curves in Fig. 5(a), where  $A, B,$  and  $T_0$  are the fitting constants.  $T_0$  is the NI phase transition temperature of the LC phase in the raw mixture (vertical solid line). As PPIPS progressed ( $m > 0$ ), the thermoresponse of  $S_{LC}$  changed from the power-law function to the sigmoid function, as shown in Figs. 5(b) and 5(c); in other words,  $S_{LC}$  approached constant nonzero values as  $\tau$  increased and decreased away from the sigmoid inflection point. The  $\tau$  dependence of  $S_{LC}$  was fitted here by a Boltzmann sigmoid

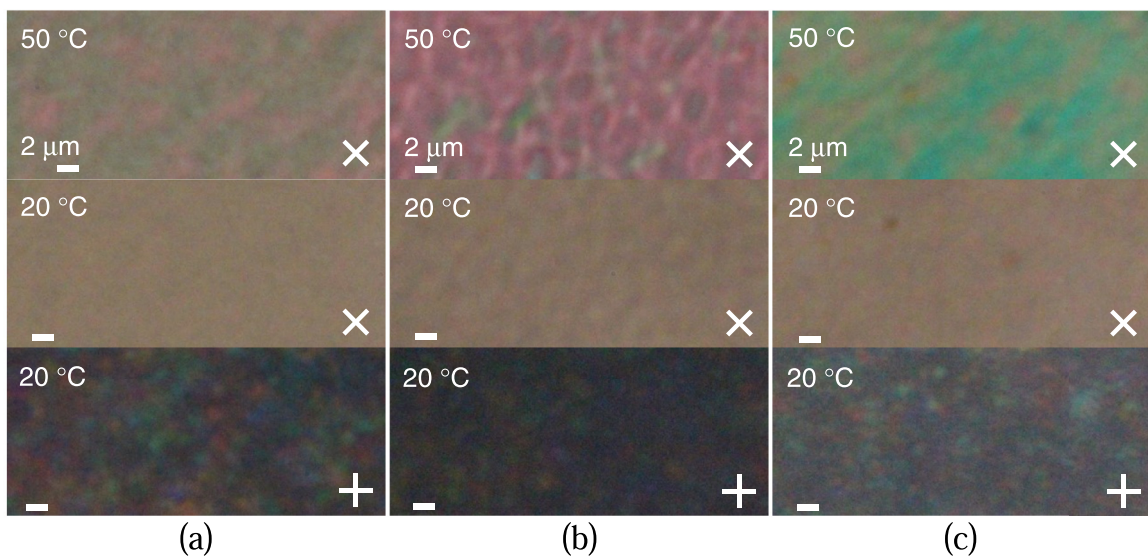


FIG. 3. Polarizing optical microscopy images of PNLCs prepared from mixtures: (a)  $\phi = 0.64,$  (b)  $0.70,$  and (c)  $0.80,$  observed at XN state with polarizing azimuths of  $\pm 45^\circ$  (upper and middle images) and  $0^\circ/90^\circ$  (lower images) from direction of rubbing treatment, where the direction is horizontal in the images. Lower and middle images were measured at 20 °C and upper images were at 50 °C. Cross symbols indicate the polarizing azimuths of two polarizers sandwiching the samples. Scale bars indicate 2  $\mu\text{m}$ .

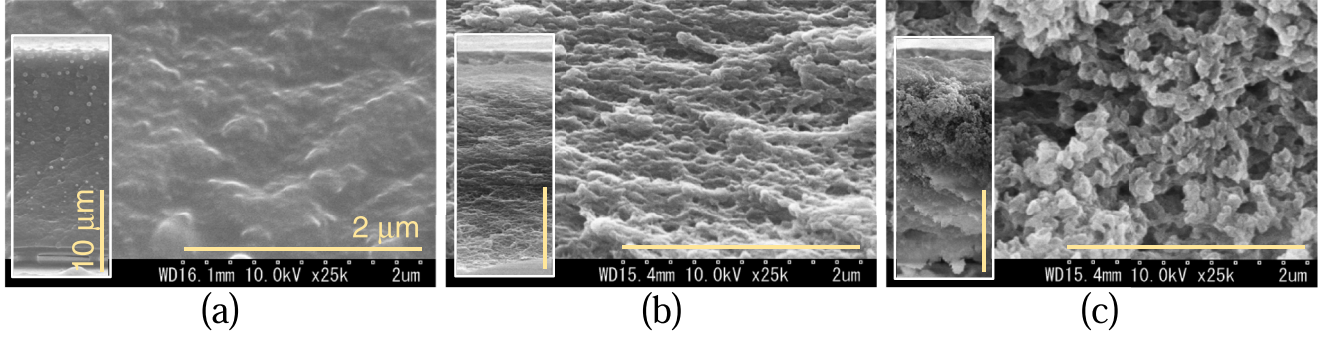


FIG. 4. SEM images of cross section of PNLCs prepared from mixtures: (a)  $\phi = 0.64$ , (b)  $0.70$ , and (c)  $0.80$ , after rinsing LCs from surface. Scale bars indicate  $2 \mu\text{m}$ . The insets are the overview of the cross section from top to bottom surfaces, where scale bars indicate  $10 \mu\text{m}$ .

function of  $\tau$ ,

$$S_{\text{LC}} = \frac{A_L - A_H}{1 + e^{(\tau - T_0)/\Delta T}} + A_H, \quad (7)$$

which has asymptotic curves to  $A_L$  and  $A_H$  with a drop and rise in temperature, respectively.  $T_0$  in Eq. (7) is the temperature of the inflection point, and  $\Delta T$  is a constant that determines the steepness of sigmoid change. The temperatures characterizing the transition behavior in the sigmoid curve can be expressed as  $(T_0 - 2\Delta T)$ ,  $T_0$ , and  $(T_0 + 2\Delta T)$ , which were obtained by the intersections of  $A_L$  and  $A_H$  with the tangent at the sigmoid inflection point (three vertical solid lines).

The  $\tau$  dependence of  $S_{\text{LC}}$  was examined at different stages of polymerization ( $m$ ). Figure 6 shows  $S_{\text{LC}}$  as a function of  $\tau$  and  $m$  at three different  $\phi$ .  $S_{\text{LC}}$  at  $\tau$  above  $T_0$  was zero before polymerization ( $m = 0$ ), and monotonically increased away from zero with increasing  $m$ . The transition temperature ( $T_0$ ) gradually decreased while the temperature range ( $4\Delta T$ ) of the transition in  $S_{\text{LC}}$  increased as  $m$  increased, as shown by the three solid black lines, where  $4\Delta T$  corresponds to the difference between the top and bottom lines. Comparing the  $\tau$  dependence of  $S_{\text{LC}}$  between different  $\phi$ , as shown in Figs. 6(a)–6(c),  $T_0$ ,  $4\Delta T$ , and the high-temperature  $S_{\text{LC}}$  at the end stage of polymerization were smaller for the samples with larger  $\phi$ .

$\Delta n_{\text{PNLC}}$  was measured as a function of  $\tau$  at different  $m$ . Figures 7(a)–7(c) show  $\Delta n_{\text{PNLC}}$  as a function of  $\tau$ , at  $m = 0, 0.55$ , and  $0.78$ , respectively, for  $\phi = 0.70$ . Before PPIPS ( $m = 0$ ),  $\Delta n_{\text{PNLC}}$  rapidly decreased and reached zero as  $\tau$  increased. This decrease is in the same way as it in typical nematic LCs and was fitted to a power-law function of  $\tau$ ,

$$\Delta n_{\text{PNLC}} = a(\tau_0 - \tau)^b, \quad (8)$$

as shown by the solid black curves in Fig. 7(a), where  $a$ ,  $b$ , and  $\tau_0$  are the fitting constants. As PPIPS progressed ( $m > 0$ ), the thermoresponse of  $\Delta n_{\text{PNLC}}$  changed from the power-law function to the sigmoid function, as shown in Figs. 7(b) and 7(c); in other words,  $\Delta n_{\text{PNLC}}$  approached constant nonzero values, as  $\tau$  increased and decreased away from the inflection point. The  $\tau$  dependence of  $\Delta n_{\text{PNLC}}$  was fitted here by a Boltzmann sigmoid function of  $\tau$ ,

$$\Delta n_{\text{PNLC}} = \frac{a_L - a_H}{1 + e^{(\tau - \tau_0)/\Delta\tau}} + a_H, \quad (9)$$

which is asymptotic to  $a_L$  and  $a_H$  with a drop and rise in temperature, respectively.  $\tau_0$  in Eq. (9) is the temperature of the inflection point and  $\Delta\tau$  is a constant that determines the steepness of the sigmoid change. The temperatures characterizing the transition behavior can be expressed as  $(\tau_0 - 2\Delta\tau)$ ,  $\tau_0$ , and  $(\tau_0 + 2\Delta\tau)$ , which were obtained from the intersections of  $a_L$  and  $a_H$  with the tangent at the sigmoid inflection point.  $\tau_0$  was

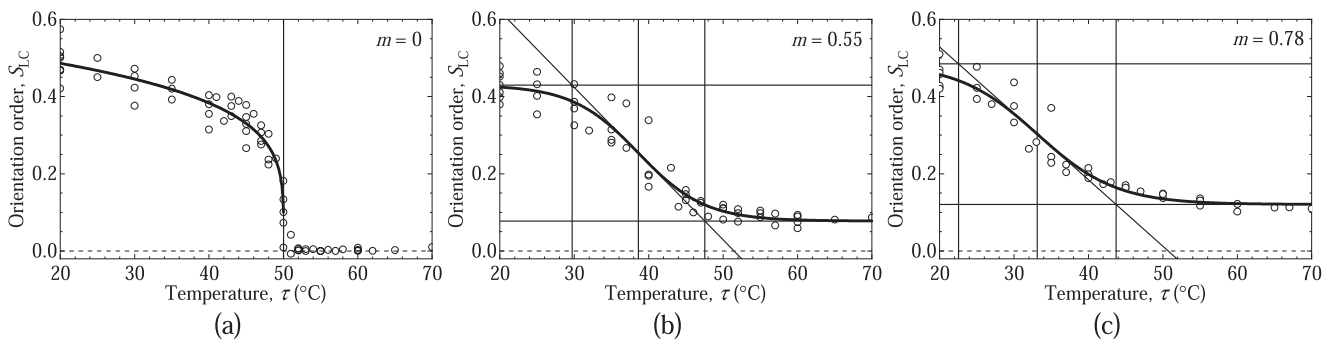


FIG. 5. Molecular orientation order of LCs in PNLCs prepared from mixture  $\phi = 0.70$ , as a function of temperature, at three different stages of the degree of conversion: (a)  $m = 0$ , (b)  $0.55$ , and (c)  $0.78$ . Solid thick curves are fitting functions, that is, a power-law function in (a) and Boltzmann sigmoid function in (b) and (c). Vertical solid line in (a) indicates  $\tau = T_0$  in Eq. (6), and those in (b) and (c) indicate  $\tau = (T_0 - 2\Delta T)$ ,  $T_0$ , and  $(T_0 + 2\Delta T)$  in Eq. (7). Horizontal solid lines in (b) and (c) indicate asymptotes at  $\tau = \pm\infty$ , and oblique solid line is tangent at  $\tau = T_0$  in Eq. (7).

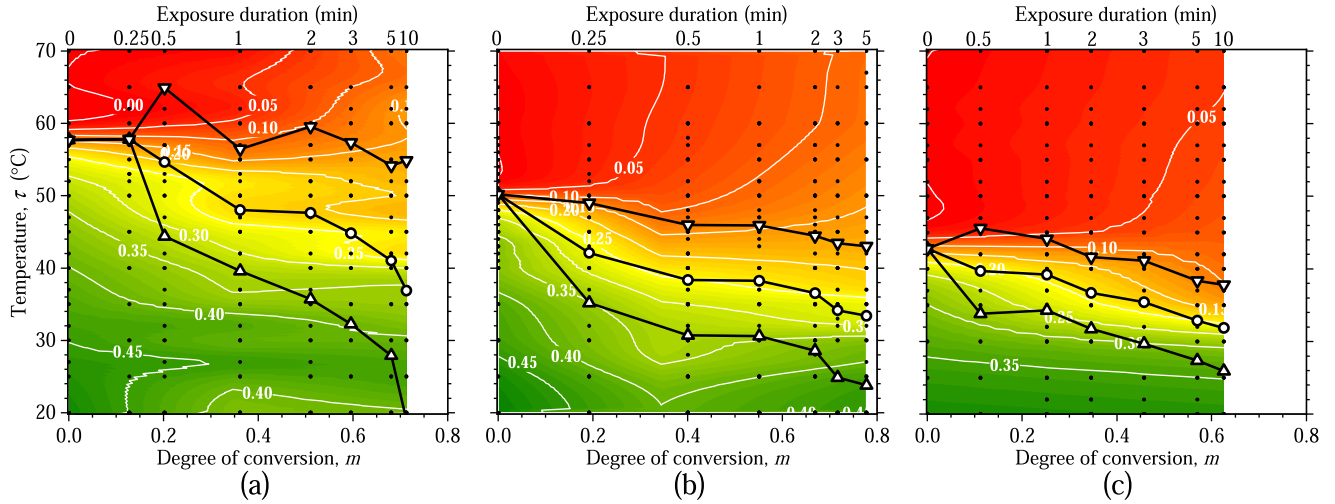


FIG. 6. Contour maps of molecular orientation order ( $S_{LC}$ ) of LCs as function of degree of conversion and temperature, for PNLCS prepared from mixtures: (a)  $\phi = 0.64$ , (b)  $0.70$ , and (c)  $0.80$ . Solid lines with circles indicate  $T_0$  in Eqs. (6) and (7), and those with upward and downward triangles indicate  $(T_0 - 2\Delta T)$  and  $(T_0 + 2\Delta T)$  in Eq. (7). Black dots are measurement points. Upper abscissa expresses photoexposure duration.

found to be higher than  $T_0$  at every  $m$ , as indicated by the vertical solid and dashed lines in the figures.

The  $\tau$  dependence of  $\Delta n_{PNLC}$  was examined at different  $m$ . Figure 8 shows  $\Delta n_{PNLC}$  as a function of  $\tau$  and  $m$  at three different  $\phi$ .  $\Delta n_{PNLC}$  at  $\tau$  above  $\tau_0$  was zero before polymerization ( $m = 0$ ), and monotonically increased away from zero with increasing  $m$ . The transition temperature ( $\tau_0$ ) gradually decreased while the temperature range ( $4\Delta\tau$ ) of the transition in  $\Delta n_{PNLC}$  increased as  $m$  increased, as shown by the three solid black lines. This temperature dependence is similar to that of  $T_0$ , but  $\tau_0$  was higher than  $T_0$  throughout PPIPS. Comparing the  $\tau$  dependence of  $\Delta n_{PNLC}$  between different  $\phi$ , as shown in Figs. 8(a)–8(c),  $\tau_0$ ,  $4\Delta\tau$ , and the high-temperature  $\Delta n_{PNLC}$  at the end stage of polymerization were smaller for the samples with larger  $\phi$ .

The low- and high-temperature values of  $S_{LC}$  were obtained using Eqs. (6) or (7), and are shown as functions of  $m$  in Fig. 9. If using Eq. (6), the low-temperature  $S_{LC}$  was set to the value in Eq. (6) at the lowest measurement temperature

(20 °C), and the high-temperature  $S_{LC}$  was set to zero. If using Eq. (7),  $A_L$  and  $A_H$  were estimated from the limit values of  $S_{LC}$  as the low- and high-temperature  $S_{LC}$ , respectively. Low- and high-temperature values of  $S_{RM}$  were estimated from  $S_{LC}$  and  $\Delta n_{PNLC}$  using

$$S_{RM} = k_{RM} \frac{\Delta n_{PNLC} - \phi_v(S_{LC}/k_{LC})}{1 - \phi_v}, \quad (10)$$

which was obtained by solving the simultaneous equations of Eqs. (1), (2), and (4). The low-temperature  $S_{RM}$  was determined using Eq. (10), with  $S_{LC} = A_L$  and  $\Delta n_{PNLC} = a_L$  in Eqs. (7) and (9), and  $S_{LC}$  and  $\Delta n_{PNLC}$  at 20 °C in Eqs. (6) and (8), respectively. The high-temperature  $S_{RM}$  was determined using Eq. (10) with  $S_{LC} = A_H$  and  $\Delta n_{PNLC} = a_H$  or  $S_{LC} = 0$  and  $\Delta n_{PNLC} = 0$  in Eqs. (6) and (8), respectively. As shown in Figs. 9(a)–9(c), the low-temperature  $S_{LC}$  was constant, independent of  $m$  and  $\phi$ . The high-temperature  $S_{LC}$  was zero at  $m = 0$  and monotonically increased with increasing  $m$ . The high-temperature  $S_{LC}$  at the end stages of PPIPS was smaller

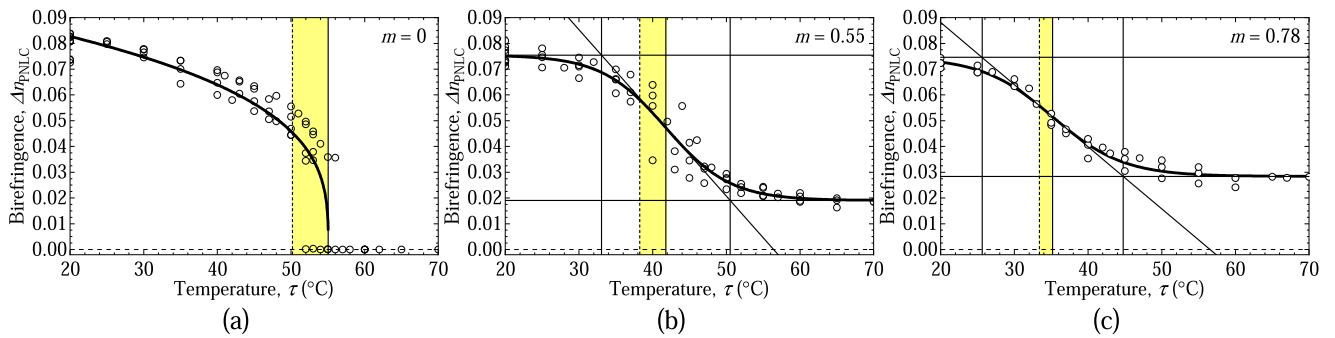


FIG. 7. Birefringence of PNLCS prepared from mixture  $\phi = 0.70$ , as a function of temperature, at three different stages of the degree of conversion: (a)  $m = 0$ , (b)  $0.55$ , and (c)  $0.78$ . Thick solid curves are the fitting function, that is, a power-law function in (a) and Boltzmann sigmoid function in (b) and (c). Vertical solid line in (a) indicates  $\tau = \tau_0$  in Eq. (8), and those in (b) and (c) indicate  $\tau = (\tau_0 - 2\Delta\tau)$ ,  $\tau_0$ , and  $(\tau_0 + 2\Delta\tau)$  in Eq. (9). Horizontal solid lines in (b) and (c) indicate asymptotes at  $\tau = \pm\infty$ , and oblique solid line is tangent at  $\tau = \tau_0$  in Eq. (9). Vertical dashed lines are  $T_0$  in Eqs. (6) and (7) after Fig. 5.

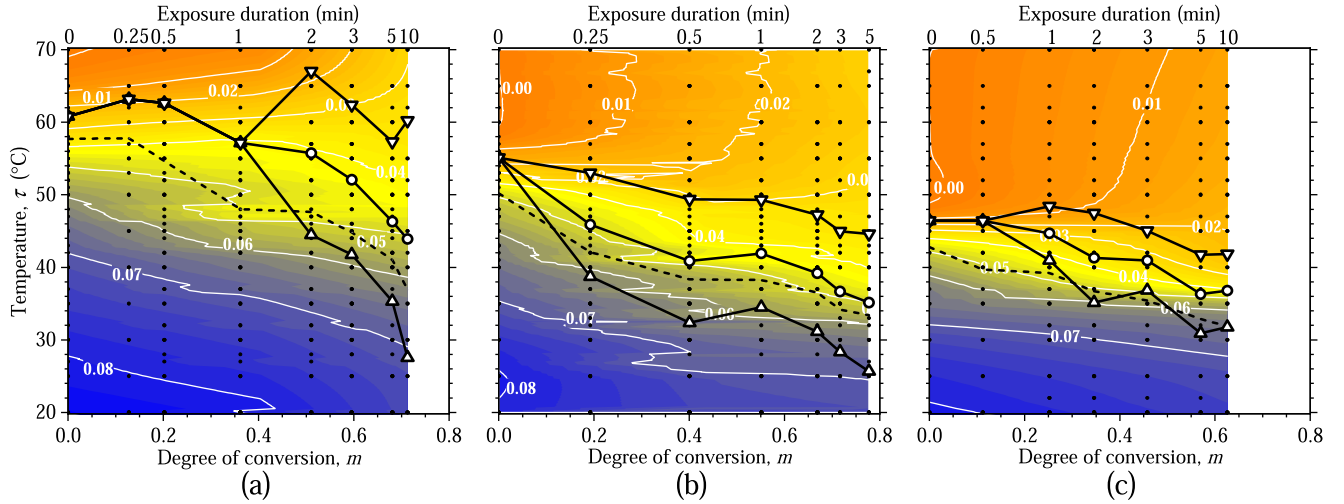


FIG. 8. Contour maps of birefringence ( $\Delta n_{\text{PNLC}}$ ) as a function of the degree of conversion and temperature, for PNLCs prepared from mixtures: (a)  $\phi = 0.64$ , (b) 0.70, and (c) 0.80. Solid lines with circles indicate  $\tau_0$  in Eqs. (8) and (9), and those with upward and downward triangles indicate  $(\tau_0 - 2\Delta\tau)$  and  $(\tau_0 + 2\Delta\tau)$  in Eq. (9), respectively. Dashed lines are  $T_0$  in Eqs. (6) and (7) after Fig. 6. Black dots are measurement points. Upper abscissa expresses photoexposure duration.

at larger  $\phi$ .  $S_{\text{RM}}$  thermoresponsively changes between nonzero and zero at  $m = 0$ . The magnitude of the thermoresponsive change in  $S_{\text{RM}}$  decreased with increasing  $m$  but did not become zero even at the end stages of PPIPS.

#### IV. DISCUSSION

The principal results follow: (i)  $T_0 < \tau_0$  throughout PPIPS. (ii) When  $m = 0$ ,  $S_{\text{LC}}$  decreases as a power-law function of  $\tau$  and clearly falls to zero at  $\tau = T_0$ . (iii) As  $m$  increases, the  $\tau$  dependence of  $S_{\text{LC}}$  becomes sigmoidal.  $T_0$  decreases and  $4\Delta T$  increases. Therefore, (iv)  $S_{\text{LC}}$  decreases to a limit greater than zero as  $\tau$  increases above  $T_0$ . (v) The thermoresponsive variation of  $S_{\text{RM}}$  gradually decreases as  $m$  increases. The high-temperature  $S_{\text{RM}}$  increases, whereas the low-temperature  $S_{\text{RM}}$  does not change significantly.

LCs belonging to PNLCs are thermally transformed in molecular orientation while being influenced by RMs

surrounding the LCs, and vice versa. The thermoresponsive change in orientation order of LCs and RMs before, during, and after PPIPS are shown in Fig. 10, where the figure two-dimensionally expresses the PPIPS and the orientation ordering that actually progress in three dimensions. At every stage of PPIPS, LCs and RMs are uniaxially ordered in molecular orientation at low temperatures and are nonuniformly transformed to disordered states with increasing temperature, as follows: First, LCs become disordered and subsequently RMs also do, but as PPIPS progresses, the low-temperature ordered state becomes less distinguishable from the high-temperature disordered state. For uniform mixtures before PPIPS, the transformation between the ordered and disordered states clearly appears at  $\tau$  of  $T_0$  and  $\tau_0$  [Fig. 10(a)]. As LCs are nonuniformly aggregated in the progress of PPIPS, some LCs become more mobile and some become less mobile in response to temperature than the LCs before PPIPS. How does the mobility of LCs and RMs vary with the progress

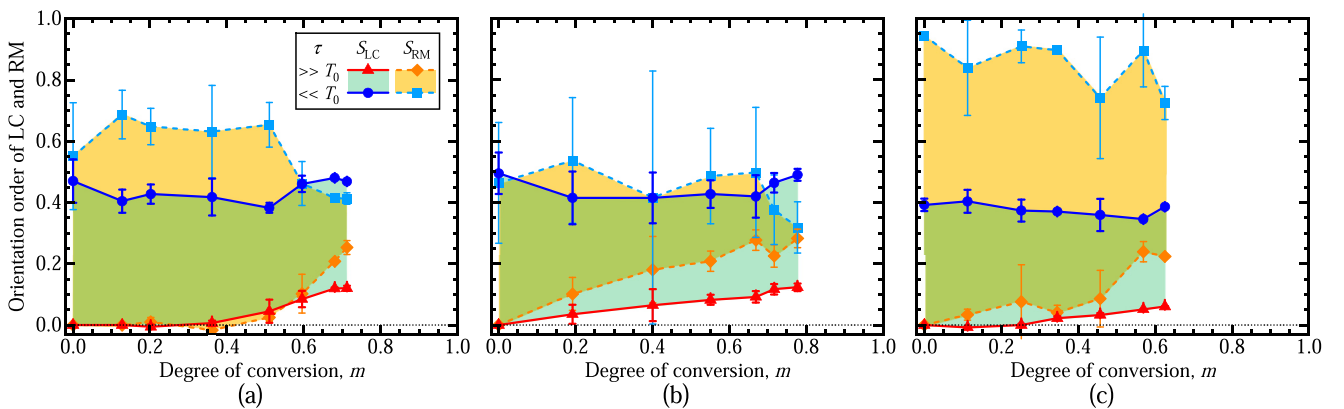


FIG. 9. Molecular orientation order of LCs ( $S_{\text{LC}}$ ) and RMs ( $S_{\text{RM}}$ ) at temperatures ( $\tau$ ) far below and above the transition temperature ( $T_0$ ), as a function of degree of conversion ( $m$ ), for PNLCs prepared from mixtures: (a)  $\phi = 0.64$ , (b) 0.70, and (c) 0.80. Symbols with solid and dashed lines indicate  $S_{\text{LC}}$  and  $S_{\text{RM}}$ .

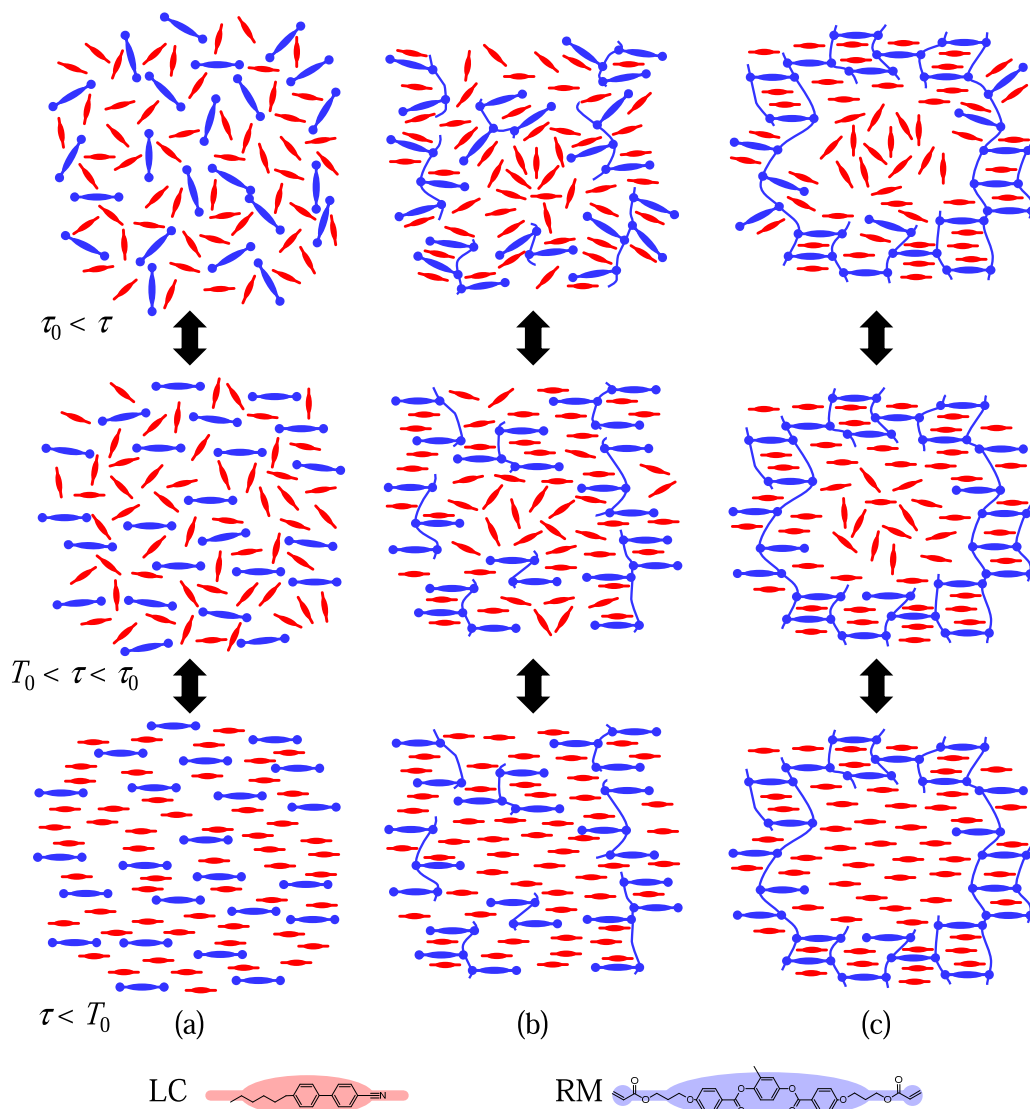


FIG. 10. Thermoresponsive change in orientation order of LCs (short red bars) and RMs (long blue bars) at different stages of PPIPS: (a) incipient, (b) middle, and (c) nearly end stages. Lower, middle, and upper figures indicate the orientation order at temperatures below  $T_0$ , between  $T_0$  and  $\tau_0$ , and above  $\tau_0$ , respectively. Polymerization of RMs is expressed by thin blue curves connecting long blue bars. Note that the PPIPS and orientation ordering are two-dimensionally expressed although they actually progress in three dimensions.

of PPIPS? The results of the temperature dependence of  $S_{LC}$  and the phase separation configuration suggest a microscopic picture of LC and RM behaviors during PPIPS [Figs. 10(b) and 10(c)]. As the PPIPS progresses, LCs located in LC-rich domains become thermally mobile, whereas LCs located in RM-rich domains become immobile. RMs at incipient stages of PPIPS are thermally transformed in orientation order. The thermoresponsive mobility of RMs is related to openness of the polymer structures (Fig. 11), such as rugged, reticular, and grainy forms, as observed by SEM, and additionally to the existence of the residual unreacted RMs, as found in the degree of conversion.

## V. CONCLUSIONS

The thermoresponsive mobility of nematic liquid crystals and main-chain ester diacrylate reactive mesogens

were extensively studied by quantitative examination of the thermal transformation of the molecular orientation order throughout photopolymerization-induced phase separation from raw mixtures to polymer network liquid crystals. These comprehensive results provide a fundamental but different approach to phase transition dynamics in ternary systems possessing polymerizable and nonpolymerizable anisotropic molecules during polymerization-induced phase separation. LCs and RMs were found to affect each other's thermoresponsive mobility nonuniformly, depending on the progress of PPIPS. The thermal transformation of the molecular orientation was uniform at the incipient stage of PPIPS, whereas it became nonuniform with the progress in PPIPS, that is, some molecules became more mobile and some became less mobile. The knowledge here is informative not only for soft-matter physics, namely, to gain a microscopic insight into miscibility (phase separation) and to discuss more elaborate



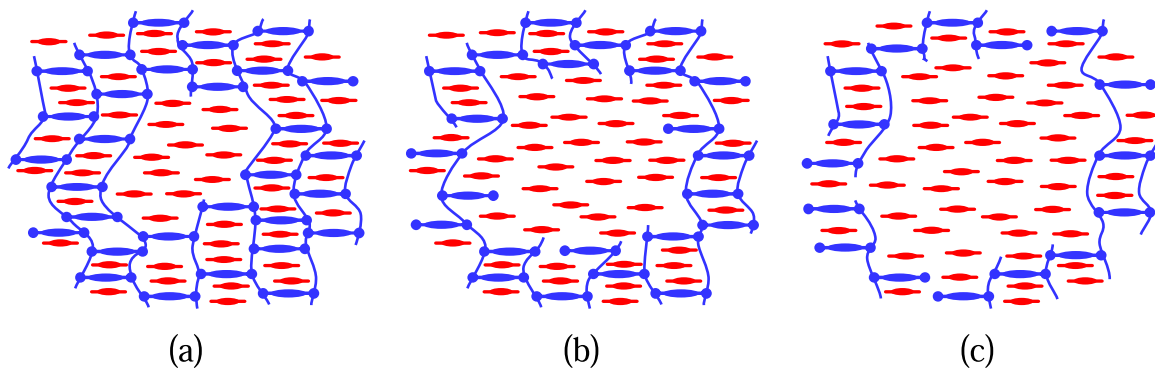


FIG. 11. PNLC structures co-ordered in molecular orientation of LCs (short red bars) and RMs (long blue bars) with different openess, prepared at (a) low, (b) middle, and (c) high compositional ratios ( $\phi$ ) of LCs in the raw mixture. Note that the structures are two-dimensionally expressed although they are three dimensional.

composite systems, but also for technological applications to develop stimuli-responsive PNLCs with faster and greater performances.

#### ACKNOWLEDGMENT

This work was partly supported by JSPS KAKENHI, Grants No. 19K03779 and No. 20K04632.

- 
- [1] C. Serbutoviez, J. G. Kloosterboer, H. M. J. Boots, and F. J. Touwslager, Polymerization-induced phase Separation. 2. Morphology of polymer-dispersed liquid crystal thin films, *Macromol.* **29**, 7690 (1996).
- [2] R. T. Pogue, L. V. Natarajan, S. A. Siwecki, V. P. Tondiglia, R. L. Sutherland, and T. J. Bunning, Monomer functionality effects in the anisotropic phase separation of liquid crystals, *Polymer* **41**, 733 (2000).
- [3] N. Kim, H. Lam, and T. Kyu, Photochromism and photopolymerization induced mesophase transitions in mixtures of spiropyran and mesogenic diacrylate, *J. Phys. Chem. B* **114**, 16381 (2010).
- [4] P. S. Drzaic, *Phase Separation in the Binodal and Spinodal Regime. Liquid Crystal Dispersions*, Series on Liquid Crystals (World Scientific, Singapore, 1995), Vol. 1, pp. 81–88.
- [5] H. Dai, L. Chen, B. Zhang, G. Si, and Y. J. Liu, Optically isotropic, electrically tunable liquid crystal droplet arrays formed by photopolymerization-induced phase separation, *Opt. Lett.* **40**, 2723 (2015).
- [6] H. Peng, L. Yu, G. Chen, Z. Xue, Y. Liao, J. Zhu, X. Xie, I. I. Smalyukh, and Y. Wei, Liquid crystalline nanocolloids for the storage of electro-optic responsive images, *ACS Appl. Mater. Interfaces* **11**, 8612 (2019).
- [7] H. Kakiuchida, A. Matsuyama, and A. Ogiwara, Normal- and reverse-mode thermoresponsive controllability in optical attenuation of polymer network liquid crystals, *ACS Appl. Mater. Interfaces* **11**, 19404 (2019).
- [8] H. Kakiuchida, M. Kabata, T. Matsuyama, and A. Ogiwara, Thermoresponsive reflective scattering of meso-scale phase separation structures of uniaxially orientation-ordered liquid crystals and reactive mesogens, *ACS Appl. Mater. Interfaces* **13**, 41066 (2021).
- [9] R. R. Deshmukh and M. K. Malik, Effect of temperature on the optical and electro-optical properties of poly(methyl methacrylate)/E7 polymer-dispersed liquid crystal composites, *J. Appl. Polym. Sci.* **109**, 627 (2008).
- [10] P. Song, Y. Gao, F. Wang, L. Zhang, H. Xie, Z. Yang, and H. Yang, Studies on the electro-optical and the light-scattering properties of PDLC films with the size gradient of the LC droplets, *Liq. Cryst.* **42**, 390 (2015).
- [11] D. Jayoti, P. Malik, and A. Singh, Analysis of morphological behaviour and electro-optical properties of silica nanoparticles doped polymer dispersed liquid crystal composites, *J. Mol. Liq.* **225**, 456 (2017).
- [12] L. Zhang, Y. Liu, Z. Shi, T. He, X. Gong, P. Geng, Z. Gao, and Y. Wang, Effects of alkyl chain length of monomer and dye-doped type on the electro-optical properties of polymer-dispersed liquid crystal films prepared by nucleophile-initiated thiol-ene click reaction, *Liq. Cryst.* **47**, 658 (2020).
- [13] L. Corvazier and Y. Zhao, Induction of liquid crystal orientation through azobenzene-containing polymer networks, *Macromol.* **32**, 3195 (1999).
- [14] D. Nwabunma, H.-W. Chiu, and T. Kyu, Theoretical investigation on dynamics of photopolymerization-induced phase separation and morphology development in nematic liquid crystal/polymer mixtures, *J. Chem. Phys.* **113**, 6429 (2000).
- [15] S. Meng, T. Kyu, L. V. Natarajan, V. P. Tondiglia, R. L. Sutherland, and T. J. Bunning, Holographic photopolymerization-induced phase separation in reference to the phase diagram of a mixture of photocurable monomer and nematic liquid crystal, *Macromol.* **38**, 4844 (2005).
- [16] S. Blonski, W. Brostow, D. A. Jonah, and M. Hess, Solubility and miscibility in ternary systems: Polymer liquid crystal + flexible polymer + solvent, *Macromol.* **26**, 84 (1993).
- [17] H. M. J. Boots, J. G. Kloosterboer, C. Serbutoviez, and F. J. Touwslager, Polymerization-induced phase separation. 1. Conversion-phase diagrams, *Macromol.* **29**, 7683 (1996).
- [18] T. Kyu and H.-W. Chiu, Morphology development during polymerization-induced phase separation in a polymer dispersed liquid crystal, *Polymer* **42**, 9173 (2001).
- [19] T. Kyu, D. Nwabunma, and H.-W. Chiu, Theoretical simulation of holographic polymer-dispersed liquid-crystal films via

- pattern photopolymerization-induced phase separation, *Phys. Rev. E* **63**, 061802 (2001).
- [20] A. Matsuyama and T. Ueda, Phase diagrams of binary mixtures of liquid crystals and rodlike polymers in the presence of an external field, *J. Chem. Phys.* **136**, 224904 (2012).
- [21] S. Anjali and R. Pratibha, Cellular structures arising from viscoelastic phase separation in binary mixtures of thermotropic liquid crystals, *Soft Matter* **13**, 2330 (2017).
- [22] M. T. Islam, T. Kamal, T. Shin, B. Seong, and S.-Y. Park, Self-assembly of a liquid crystal ABA triblock copolymer in a nematic liquid crystal solvent, *Polymer* **55**, 3995 (2014).
- [23] E. Ouskova, L. De Sio, R. Vergara, T. J. White, N. Tabiryan, and T. J. Bunning, Ultra-fast solid state electro-optical modulator based on liquid crystal polymer and liquid crystal composites, *Appl. Phys. Lett.* **105**, 231122 (2014).
- [24] N. Kim and T. Kyu, Phase equilibria and photopolymerisation-induced phase transitions of mesogenic diacrylate monomer and low molecular mass liquid crystal mixture, *Liq. Cryst.* **39**, 745 (2012).
- [25] M. Sandmann and A. Würflinger, PVT measurements on 4'-n-hexyl-biphenyl-4-carbonitrile (6CB) and 4-n-heptyl-biphenyl-4-carbonitrile (7CB) up to 300 MPa, *Z. Naturforsch.* **53a**, 233 (1998).
- [26] The specific gravities of 6CB and RM257 were calculated to be  $1.02 \pm 0.1$  and  $1.219 \pm 0.06$  g/cm<sup>3</sup>, respectively, using Advanced Chemistry Development Software V11.02.
- [27] F. Basile, F. Bloisi, L. Vicari, and F. Simoni, Optical phase shift of polymer-dispersed liquid crystals, *Phys. Rev. E* **48**, 432 (1993).
- [28] A. R. Noble-Luginbuhl, R. M. Blanchard, and R. G. Nuzzo, Surface effects on the dynamics of liquid crystalline thin films confined in nanoscale cavities, *J. Am. Chem. Soc.* **122**, 3917 (2000).
- [29] A. Andrejeva, A. M. Gardner, W. D. Tuttle, and T. G. Wright, Consistent assignment of the vibrations of symmetric and asymmetric para-disubstituted benzene molecules, *J. Mol. Spectrosc.* **321**, 28 (2016).
- [30] I. M. Ward, Determination of molecular orientation by spectroscopic techniques, *Adv. Polym. Sci.* **66**, 81 (1985).
- [31] D. E. Aspnes, Optical properties of thin films, *Thin. Solid Films* **89**, 249 (1982).
- [32] W. Heller, Remarks on refractive index mixture rules, *J. Phys. Chem.* **69**, 1123 (1965).
- [33] See Supplemental Material at <http://link.aps.org/supplemental/10.1103/PhysRevE.106.044704> for the experiment results to verify the reliability of the additivity of the birefringence.
- [34] K. Matsukawa, Y. Matsuura, H. Inoue, K. Hanafusa, and N. Nishioka, Development of photocuring acrylic/silica organic-inorganic hybrid for negative resists, *J. Photopolym. Sci. Technol.* **14**, 181 (2001).
- [35] N. B. Colthup, L. H. Daly, and S. E. Wiberley, in *Introduction to Infrared and Raman Spectroscopy*, 3rd ed. (Elsevier, Amsterdam, 1995), Chap. 9, pp. 289–325.